Available online at www.sciencedirect.com

ScienceDirect

Journal of Hydro-environment Research 5 (2011) 215–230

Journal of Hydro-environment Research

www.elsevier.com/locate/jher

Research paper

PIV and PTV measurements in hydro-sciences with focus on turbulent open-channel flows

Iehisa Nezu*, Michio Sanjou

Department of Civil and Earth Resources Engineering, Kyoto University, Kyoto 615-8540, Japan

Accepted 21 May 2011

Abstract

PIV is one of the most popular measurement techniques in hydraulic engineering as well as in fluid sciences. It has been applied to study various turbulent phenomena in laboratory experiments related to natural rivers, e.g., bursting phenomena near the bed, mixing layers observed at confluences, wake turbulence around dikes and piers, and so on. In these studies, PIV plays important roles in revealing the space-time structure of velocity fluctuations and coherent vortices. This review article focuses particularly on the applications of PIV to turbulent open-channel flows, which have been conducted for the past decade in Hydraulics Laboratory of Kyoto University. In Section 2, we introduce our experimental setup and PIV/PTV algorithm. In Section 3, we apply the PIV measurements to reveal turbulence characteristics and coherent structures in open-channel flows as well as in vegetated canopy flows. For complex flow situations, various applications of PIV to compound open-channel flows and wind-induced water waves are considered to reveal coherent vortices. In Section 4, we discuss some advanced PIV measurements in open-channel flows. The free-surface-elevation fluctuations and velocity components were measured simultaneously with two sets of cameras to examine phase-averaged parameters of turbulence. A multi-layer scanning PIV was developed to reveal 3D turbulence structure in compound open-channel flows. Our discriminator PIV/PTV was applied successfully to sediment-laden open-channel flows and revealed the fluid/particle interaction and the relationship between coherent structures and sediment concentration. Finally, we conducted simultaneous measurements of velocity and dye concentration with a combination of PIV and LIF in vegetated open-channel flow, which enables us to examine turbulent scalar flux of a passive contaminant.

Keywords: PIV Measurements; Open-channel flow; Turbulence; Coherent structure

1. Introduction

Flow visualizations have been extensively conducted to investigate fluid motion, vortex patterns and turbulence in the fields of fluid dynamics, aeronautical mechanics and hydraulic engineering. The development of various useful methods has enabled us to conduct quantitative flow visualizations, in which fluid motion was evaluated by examining temporal variations of dye clouds, hydrogen bubbles and tracer particles. In PIV measurements of turbulent flows, seeding particles such as polystyrene (specific density is 1.02) have been used in water, together with a laser light sheet (LLS).

Two kinds of methods have been developed to obtain velocity vectors from the sequential digital images, i.e., one is the individual particle tracking and the other is the statistical cross-correlation of sequential narrow-window images. The former is called "particle-tracking velocimetry (PTV)" and the latter "particle-image velocimetry (PIV)". Various schemes for PTV are proposed to obtain velocity distributions. It is, however, very difficult to identify particle pairs in highly concentrated particle images, and thus PTV has been limited to low-concentration particle-laden flows. This implies that the number of velocity vectors obtained in space is comparatively small in PTV measurements. In contrast, PIV follows some patterns of

* Corresponding author. Tel./fax: +81 75 383 3185.
E-mail address: Iehisa.Nezu@water.kuciv.kyoto-u.ac.jp (I. Nezu).

1570-6443/$ - see front matter
doi:10.1016/j.jher.2011.05.004

particles by using a cross-correlation function between a pair of digital images in a narrow interrogation window.

PIV provides the velocity vectors of tracer particles illuminated by planar laser light. With the advent of powerful laser light sources, high-capacity computers and digital cameras, PIV instruments and the associated data processing techniques have progressed intensively. For example, Adrian (1991) has written a comprehensive review article about PIV techniques.

One of the most significant advantages of flow-visualization techniques such as PIV/PTV is that they are non-intrusive and thus do not disturb the flow at all unlike probe measurements. Nowadays, PIV techniques have spread widely and the advanced applications are conducted in various types of complex flows although each technique may be different in many fundamental and applied research fields including fluid engineering, medical science and industry flows, e.g., see Raffel et al. (2007) and Schroeder and Willert (2008). PIV has also become one of the most popular measurement techniques in hydro-sciences, and been applied to various flow fields related to rivers and ocean systems, such as open-channel flows, mixing layers, wakes around obstacles and so on. In these studies, PIV plays a vital role in revealing the space-time structure of velocity fluctuations and coherent vortices.

Although it was difficult for earlier PIV to capture high-speed near-wall flows, the development of double-pulse lasers and high-speed cameras has enabled us to measure turbulence structure and coherent vortices in both the inner and outer layers. Adrian et al. (2000) conducted PIV measurements of turbulent boundary layers, and found that the coherent structure is likely to be composed of vortex packets, in which several hairpin vortices are aligned in the streamwise direction. They divided the boundary layer into three sub-zone with approximately uniform momentum, and revealed that the normalized thickness of the three sub-zones depended on the Reynolds number, whereas the mean velocity of each sub-zone was almost independent of the Reynolds number. Later, Tomkins and Adrian (2003) conducted PIV measurements of horizontal planes at several heights in the buffer layer and the log-law layer to make three-dimensional (3D) examinations of boundary-layer structure. Their study supported the vortex packet model proposed by Adrian et al. (2000). Hurther et al. (2007) recognized that these coherent structures are also observed in the outer layers of open-channel flows. In the same manner, Sanjou and Nezu (2010) examined the effects of water waves on hairpin-vortex generation and decay processes using PIV measurements and Adrian et al. (2000)'s method.

It is well known that large-scale circulations and wake vortices such as the Karman vortex contribute significantly to hydrodynamic structures around dikes, aquatic vegetation, bridge piers and side cavities. For example, Kadota et al. (2007) conducted PTV measurements of flows around emergent tandem cylinders and captured both small- and large-scale vortex patterns. Further, one of PIV advantages is the comparatively easy extension to the large-scale fluid field in nature. Examples of this type include the visualization techniques for free-surface flow in rivers. Fujita et al. (1998) dubbed the "LSPIV" (large-scale PIV) as the most of measurements were taken over surfaces much larger than those in laboratory PIV. Further, Fujita et al. (2009) stressed an importance of LSPIV in river flow information.

Compound open-channel flows consist of two-stage channels, i.e., the main-channel and floodplains, as often observed in rivers during floods. Coherent horizontal vortices appear near the junction, and promote the transverse exchanges of mass and momentum between the main-channel and floodplains. A horizontal vortex was first visualized by Sellin (1964) using the aluminum-powder method. Later, Nezu et al. (1999b) found from PIV measurements that a twin-vortex structure, which consists of counter-rotating vortex pairs, appeared as the water depth reached 1.5 times the floodplain height. Meandering compound open-channel flow is also an area of high interest in river engineering. Sanjou and Nezu (2009) have developed a multi-layer scanning PIV system to reveal such complex flow structure. They found that significant secondary currents and horizontal vortices were generated due to an interaction between meandering inbank main-channel flow and straight overbank floodplain flow.

The other advantage of PIV is a possibility of simultaneous measurements between velocity components and scalar variables such as dissolved gas concentration and dye concentration. For example, Herlina and Jirka (2008) have successfully conducted simultaneous measurements of velocity and dissolved oxygen (DO) concentration using a combination between PIV and laser-induced fluorescence (LIF) near the air–water interface induced by oscillating grid turbulence. On the other hand, Okamoto et al. (2010) have conducted simultaneous measurements of velocity and dye concentration using a combination between PIV and LIF in vegetated canopy open-channel flow. Such an LIF provides a non-intrusive method of high-resolution measurements of mass concentration in water flows.

According to our experiences of PIV/PTV measurements, the present review article focuses on the application of PIV/PTV to turbulent open-channel flows, which have been conducted for the past decade in Hydraulics Laboratory of Kyoto University. In Section 2, we introduce our experimental setup and PIV/PTV algorithm. In particular, a discrimination method between fluid and sediment particles is proposed and discussed. In Section 3, we apply the PIV measurements to reveal turbulence characteristics and coherent structures over smooth and rough (vegetation) beds in open-channel flows. For complex flow situations, various applications of PIV to compound open-channel flows and wind-induced water waves are treated and discussed to reveal coherent vortices.

In Section 4, we discuss some advanced PIV measurements in open-channel flows. The free-surface-elevation fluctuations and velocity components are measured simultaneously with two sets of cameras to examine phase-averaged parameters of turbulence. Three-dimensional (3D) PIV is one of the most innovative techniques to be developed in the fluid measurement community, e.g., see recent review articles by Scarano (2010) and Ruck (2011). We have developed a multi-layer scanning PIV and applied it to compound open-channel flows. Our discriminator PIV/PTV was applied successfully to sediment-laden open-channel flows and revealed a fluid/

particle interaction. Finally, simultaneous measurements of velocity and dye concentration were conducted with a combination of PIV and LIF in vegetated open-channel flow to examine mass transport phenomena.

2. Experimental procedures

2.1. PIV setup

Fig. 1 shows a typical PIV configuration for water flume, in which a high-sensitivity CCD/CMOS camera and laser light source are required. A laser beam is converted to a planar sheet of light, i.e., laser light sheet (LLS), via a cylindrical lens. The LLS should be as thin as possible to remove the influences of out-of-plane velocities. The LLS is generally projected into the fluid volume vertically or horizontally in laboratory measurements. Two components of instantaneous velocity are evaluated from images of tracer particles illuminated by the LLS using the relevant PIV algorithm.

x, y and z are the streamwise, vertical, and spanwise coordinates, respectively. For example, the instantaneous velocity components $(\widetilde{u} \equiv U + u, \widetilde{v} \equiv V + v)$, can be measured in Fig. 1, where the capital and small letters denote the time-averaged component and the turbulent fluctuating one, respectively. Nezu and Azuma (2004) used a 2W argon-ion laser, which was guided through an optical fiber cable and illuminated the flow vertically as a 2 mm thick LLS. This LLS was adjusted by a computer-controlled acousto-optic modulator (AOM), in which the light emission interval Δt and its duration δt were adjusted in the range $\Delta t = (1-5)$ ms and $\delta t = (0.1-0.9)$ ms, respectively (see Fig. 2). Pairs of particle images were taken by a high-sensitivity CCD camera. Nezu and Azuma (2004) used this AOM controlled LLS system (i.e., frame straddling method) in open-channel flows, as shown in Fig. 2. Two closely-spaced light pulses are generated by the AOM and thus the image pairs are obtained at every odd-frame end and even-frame beginning. A double-pulse YAG laser may be more conveniently used for the frame straddling instead of argon-ion laser with AOM. The frame straddling method can be applied to measurements of high-speed flows when the interval Δt of the frame pairs is set very small. Otherwise, we may be able to use a high-speed CMOS camera, say the frame time $\Delta t = (1-2)$ ms or (500−1000)Hz, when the LLS illumination is powerful enough to obtain good pictures.

The choice of tracer particles is one of the most significant procedures in PIV/PTV measurements. Our group, e.g. see Nezu et al. (1999b), Nezu and Azuma (2004) and Nezu and Sanjou (2008), have used Nylon-12 particles of 100 μm diameter and 1.02 specific density because these particles scatter homogeneously in water flow and are large enough to obtain good images of particles. However, Noguchi and Nezu (2009) have used much smaller-size particles of 25 μm diameter Nylon-12 for fluid tracers in order to discriminate fluid from sediment particles. The tracer particles were seeded carefully in water after coating them with a minimal amount of alcohol in order to realize a homogeneous distribution in flows.

2.2. PIV algorithm

The direct cross-correlation method (DCM) is the most popular algorithm of the PIV to obtain the instantaneous velocity vectors. The DCM detects the similarities in local patterns of brightness by cross-correlating the two images between the time Δt, e.g. see Adrian (1986). An interrogation region of $N \times N$ pixels is chosen in the first image, and then a search region is examined in the second image. The candidate point that has the largest correlation with the interrogation region of the first image is obtained automatically by using DCM. The planer velocity components $(\widetilde{u}, \widetilde{v})$ are then calculated using the position vector $(\Delta x = x_c - x, \Delta y = y_c - y)$ from the original point (x,y) toward the candidate point (x_c,y_c), as follows.

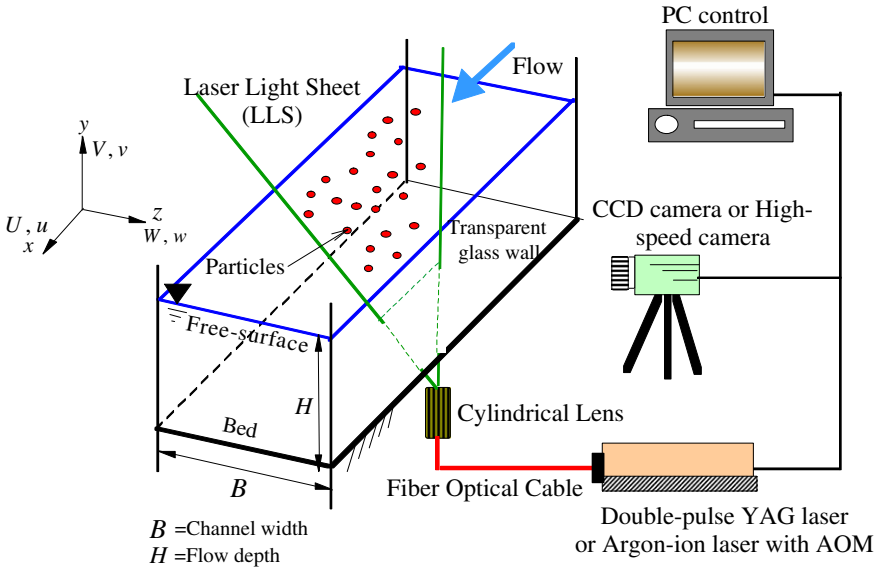

Fig. 1. Experimental setup of open-channel flow and PIV arrangements.

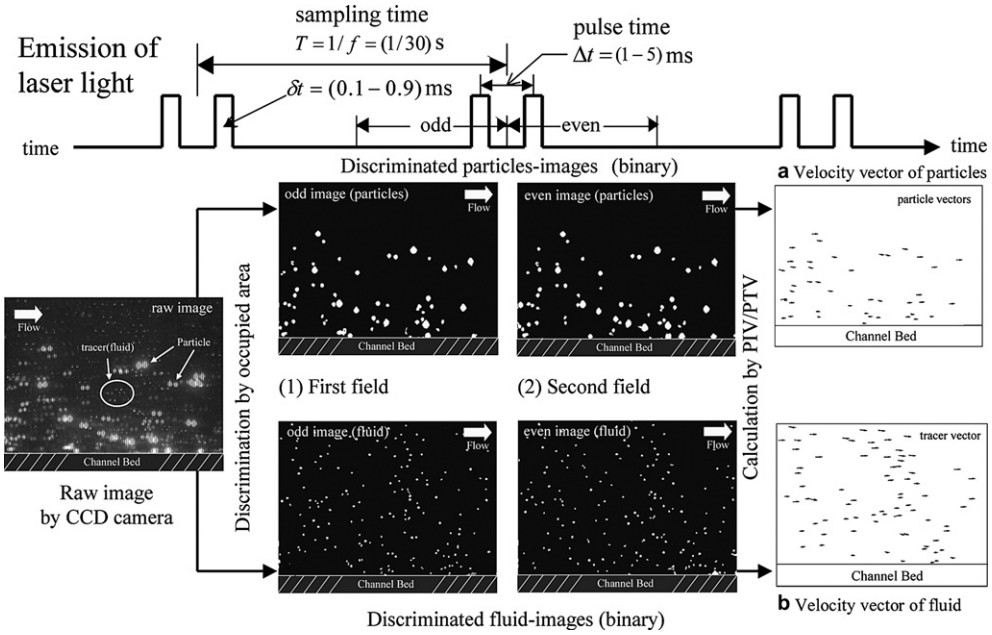

Fig. 2. Image processing between sediment particles and fluid tracers in discriminator PIV/PTV (after Nezu and Azuma, 2004).

$$\widetilde{u}(x,y) = \Delta x/\Delta t \quad \text{and} \quad \widetilde{v}(x,y) = \Delta y/\Delta t \tag{1}$$

The real peak correlation may appear close to a pixel that has the second peak. If such a peak correlation function is assumed to be Gaussian distribution, the candidate point can be evaluated at a sub-pixel location.

Because the interrogation region corresponds to the measurement-volume size of velocities, smaller interrogation regions should be used to realize higher spatial-resolution PIV. However, smaller interrogation regions may introduce more incorrect velocity vectors. It is therefore very important to choose the interrogation size reasonably by comparing PIV results with corresponding LDA data. For example, Nezu and Sanjou (2008) have chosen an interrogation size of $N = 29$ pixels in vegetated open-channel flows by comparing with corresponding LDA data, in which a sub-pixel analysis was conducted by using a Gaussian distribution.

A lot of innovative PIV software may be now available commercially and more detailed information on PIV error correlation is also available in Hart (2000).

2.3. PTV algorithm

PTV (particle tracking velocimetry) may be simple and straightforward because it tracks a target particle in space and time; the candidate point is of course determined by the position of the target particle in Eq. (1).Various algorithms such as four-time-steps model, pattern matching model, spring model and others have been proposed to identify target particles in space and time, e.g., see Kobayashi (2002). For example, Nezu et al. (1999a) conducted the four-time-steps PTV to track sand particles in open-channel flow over gravel bed. In this algorithm, a target particle was tracked in the four consecutive images by using a Kalman filter algorithm. However, it was fairly difficult to identify sand-particle trajectories near the bed in the four-time-images, because sand-particle motion was quite complicated and sand particles moving toward the bed sometimes rebounded from the bed. To overcome these difficulties, Nezu and Azuma (2004) developed a spring model PTV in sediment-laden open-channel flow, which was originally proposed by Okamoto et al. (1995). This spring model is a two-fields image algorithm, based on a pattern matching of particle cluster between two consecutive images using invisible elastic springs. It should be noted that the spring model is useful even to flow fields including particles that appear and disappear between the two consecutive images, and thus it may be powerful to apply to sediment-laden flows.

The spatial resolution of PIV is equal to the interrogation size (say, 20 to 30 pixels), whereas that of PTV corresponds to the particle size (say, 2 to 4 pixels). This implies that the dynamic spatial range of PTV may be better by one order than that of PIV. However, it should be noticed that when a lot of tracer particles (high-concentration) are released in water, it is very difficult to identify and track such a large number of tracer particles. As a result, the total number of velocity vectors obtained by PTV (dilute concentration of particles) is much smaller than that obtained by PIV.

2.4. Discrimination between fluid and sediment particles

Sediment-laden open-channel flow is one of the most complicated but most challenging flow configurations since it plays an essential role in sediment transport. This is because the sediment concentration becomes much larger closer to the bed due to gravity and thus the fluid-particle interactions are more enhanced. Further, coherent structures such as ejections and sweeps may significantly influence such fluid-particle interactions, as pointed out by Nino and Garcia (1996), Muste (2002), Nezu and Azuma (2004), and others. With the advent of the

laser Doppler anemometer (LDA) and the phase Doppler anemometer (PDA), accurate non-intrusive measurements have been possible in particle-laden flows since the 1990's.

Recent flow-visualization techniques such as PTV can be applied to measure the sediment-particle motion in space and time. The most notable advantage of PTV against LDA is the possibility of measurements of larger particles, by which the fluid-particle interactions will be able to be examined. For example, Nezu and Azuma (2004) have conducted PTV measurements of turbulence characteristics in particle-laden open-channel flows. The particle data and fluid data were separated by discriminating the occupied area sizes of particle images and water tracers on CCD camera.

Fig. 2 shows an example of a raw image and the processing images of solid particles and fluid tracer in sediment-laden open-channel flow conducted by Nezu and Azuma (2004). The raw image consists of the odd and even scanning lines. The brightness of the raw image was optimized (pre-processing), and separated into the odd and even fields with the time interval Δt. The separated images were binarized, and each particle and fluid tracer in the field was then discriminated by using a threshold value of the occupied area of particles.

The length of 1 pixel in the CCD camera corresponded to 0.03 mm (close-up picture) and 0.15 mm (overall picture) in the experiments of Nezu and Azuma (2004). The occupied area of the smallest-size sediment particle of 0.3 mm was larger than 100 pixels (close-up) and 4 pixels (overall), respectively. In contrast, the occupied area of fluid tracer of 0.1 mm was smaller than 1 pixel. Therefore, it was easy to discriminate the solid particles and fluid tracer automatically, as shown in Fig. 2. If only part of a particle was captured as the fluid tracer in the odd field and its larger part was captured as a solid particle in the even field, such data were omitted from the analysis, and vice verse in the even–odd fields. Therefore, the crosstalk of discrimination between particle and fluid would be negligibly small even in the case of the smallest-size particles, because of the very short time interval $\Delta t = 4$ ms between the odd and even fields in the experiments of Nezu and Azuma (2004).

Similar discrimination techniques between sediment particles and fluid have been developed intensively in PIV/PTV measurements to examine the fluid–particle interaction and the effects of coherent structures in sediment-laden open-channel flows, by Breugem and Uijttewaal (2006), Muste et al. (2009), Noguchi and Nezu (2009) and others.

3. Application of PIV to various open-channel flows

3.1. Open-channel turbulence near the wall

Nezu and Azuma (2004) have conducted simultaneous measurements of both the sediment particles and fluid (water) in sediment-laden open-channel flows. The sediment particle (diameter $d_p = 0.3$–1.3 mm) and fluid (tracer particle $d_p \leq 0.1$ mm, specific density $= 1.02$) were discriminated by their occupied area on images (particle-size discrimination method) as shown in Fig. 2. The sediment particle velocity was evaluated by PTV, whereas the water velocity was evaluated by PTV or PIV. Fig. 3 shows the mean velocity $U_f^+ \equiv U_f/U_*$ of fluid against the wall-unit coordinate $y^+ \equiv yU_*/\nu$, in which U_* is the friction velocity and ν is the kinematic viscosity. In clear-water (sediment-free) flow, a laser Doppler anemometer (LDA) can measure the fluid velocity accurately, and thus examine the accuracy of image-based velocimetry such as PIV and PTV. Fig. 3 compares the results of PTV and LDA in the case of CW2(bulk mean velocity $U_m = 24.6$ cm/s, flow depth $H = 5.0$ cm, Reynolds number $Re = 1.2 \times 10^4$) and CW3($U_m = 50.0$ cm/s, $H = 5.0$ cm, $Re = 2.5 \times 10^4$). The PTV data are shifted 5 units upwards in the vertical axis to avoid confusions. Fig. 3 includes the following theoretical curves.

$$U_f^+ = y^+ \text{ for viscous sublayer } \left(y^+ \leq 5\right) \tag{2}$$

$$U_f^+ = \frac{1}{\kappa}\ln y^+ + A \quad \text{for log-law layer } \left(30 \leq y^+\right) \tag{3}$$

The van Driest curve in the buffer layer $(5 \leq y^+ \leq 30)$ is also compared in Fig. 3. The PTV data are in good agreement with LDA data and the theoretical curves of Eqs. (2) and (3).

Fig. 4 shows some comparisons of Reynolds stress $-\overline{u_f v_f}/U_*^2$ against y/H. The following theoretical curve of Reynolds stress is included in Fig. 4.

$$\frac{-\overline{u_f v_f}}{U_*^2} = \left(1 - \frac{y}{H}\right) - \frac{\mathrm{d}U_f^+}{\mathrm{d}y^+} \tag{4}$$

In the case of clear-water flows (CW2 and CW3), the PTV data are compared with LDA data. Both of them are in good agreement with Eq. (4) even near the wall. In sediment-laden flows with sediment diameter $d_p = 0.5$ mm and 0.8 mm (PS series: specific density $\rho_p = 1.05$, whereas PM series: $\rho_p = 1.15$), the Reynolds stress of the fluid was measured accurately by PTV although LDA measurements could not be conducted because of laser-beam blocking by sediment particles. This may be one of

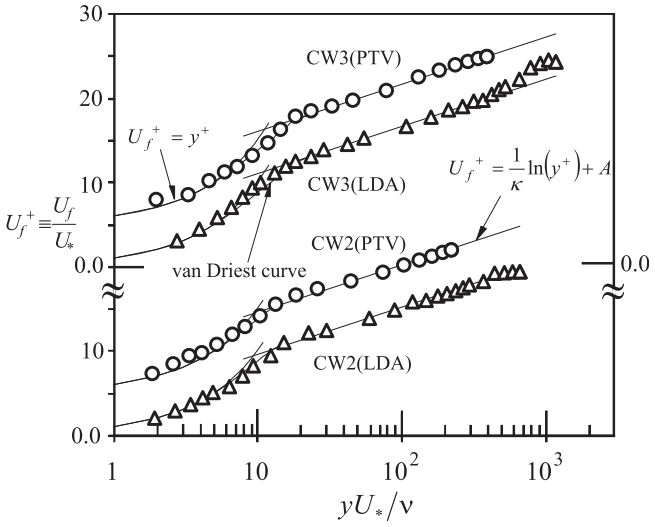

Fig. 3. Comparison of mean velocity profiles in clear-water open-channel flows measured by LDA and PTV ($U_m = 24.6$ cm/s, $H = 5.0$ cm in case CW2, and $U_m = 50.0$ cm/s, $H = 5.0$ cm in case CW3).

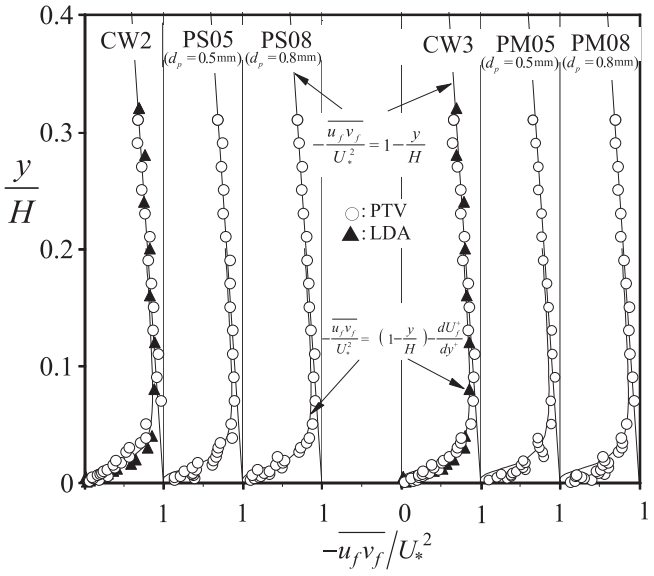

Fig. 4. Comparison of Reynolds stress distributions near the wall in sediment-laden open-channel flows.

advantages of image-based velocimetry in sediment-laden flows as compared with laser Doppler velocimetry.

Nezu and Azuma (2004) concluded from Figs. 3 and 4 that the accuracy of their PTV was sufficiently high for both the mean velocity and the second-order turbulence statistics, such as Reynolds stress, even in the near-wall region of sediment-laden open-channel flows. They examined then the relative velocity between sediment particles and fluid, and highlighted the fluid–particle interaction in relation to the ejection/sweep motion which occurs violently near the wall.

3.2. Coherent structures in open-channel flows

PIV has now become very powerful tool for studying coherent structures such as ejection and sweep motion in boundary layers and open-channel flows. This may be because PIV enables us to examine the space-time distributions of velocity vectors and evaluate the vortex structure more effectively rather than point-measurements such as LDA and acoustic Doppler velocimetry (ADV). Most of earlier studies measured the near-wall region by various flow-visualization techniques and inferred a hairpin vortex structure of bursting phenomena, as reviewed by Nezu and Nakagawa (1993). For example, Acarlar and Smith (1987) observed hairpin vortices at low Reynolds numbers by dye-injection and hydrogen-bubble techniques.

However, it had been difficult until the advent of PIV to measure coherent structures in space quantitatively, especially in the outer region of boundary layers and open-channel flows, because the main-flow velocity was too high to measure them accurately by conventional flow-visualization techniques.

Fortunately, Adrian et al. (2000) have developed an innovative PIV system (double-pulsed-laser PIV and 1320 × 1035 pixel CCD camera), and investigated the vortex structure in the outer region of boundary layers. The uncertainty with mean displacement of the tracer particles in the free-stream velocity U_∞ yielded a relative error less than 1%. They found typical hairpin vortices in the streamwise-aligned packets on the basis of moving coordinate subtracted by the relevant convection velocity U_c, say $U_c = (0.8–0.9)U_\infty$. Of particular significance is that the boundary layer can be reasonably divided into three sub-zones of uniform momentum in the moving coordinate subtracted by the convection velocity U_c. Hurther et al. (2007) found similar coherent vortex structures in the outer region of open-channel flow although they utilized a home-made acoustic Doppler velocity profiler (ADVP) instead of PIV method.

Sanjou and Nezu (2010) have conducted PIV measurements in the outer region of open-channel flow over smooth bed (channel width $B = 40$ cm, flow depth $H = 4$ cm, and maximum free-surface velocity $U_\infty = 24$ cm/s), and analyzed the coherent vortex structure in the similar manner as proposed by Adrian et al. (2000). The aspect ratio *B/H* of flume was 10 and thus fully-developed 2-D open-channel flow was realized, as pointed out by Nezu and Nakagawa (1993). Fig. 5 shows some examples of the instantaneous velocity vectors $(\widetilde{u}, \widetilde{v})$ subtracted by $U_c = 0.9U_\infty$ in the vertical channel–center plane (x-y plane) at time $t = 0$s and 0.1s. Three sub-zones are divided by (1) low-speed zone $(\widetilde{u}/U_\infty < 0.7)$, (2) middle-speed zone $(0.7 \le \widetilde{u}/U_\infty \le 0.9)$), and (3) high-speed zone $(\widetilde{u}/U_\infty > 0.9)$. The head of hairpin vortices (A, B, C and D indicated by white circle in Fig. 5, which were judged by eyes from closed streamlines of velocity vectors) appear clearly near the boundary between the zone (2) and zone (3). This zone boundary is described approximately by white dashed lines which form a zigzag pattern. That is to say, the positively-inclined packet line almost always follows a negatively-inclined one, which resembles a tent-like structure with cyclic recurrence, as pointed out by Hurther et al. (2007). Zone (1) is the near-wall region, i.e., the inner-layer structure, which has been intensively investigated by many researchers.

Of particular interest is that a violent ejection motion (indicated by white dashed circle) may occur just upstream of hairpin vortex, which infers significant interaction between the inner-layer bursting motion and the outer-layer large-scale vortical motion, as suggested by Nezu and Nakagawa (1993). As the time $t = 0.1$ s passes, the coherent packet structure which consists of hairpin vortices is convected downstream and deformed slightly. Such PIV measurements will reveal the significant interactions between the inner-layer and outer-layer coherent structures in open-channel flows.

3.3. Turbulence structure and coherent motion in vegetated open-channel flows

PIV measurements are useful to examine turbulence structure and the associated coherent motion in vegetated canopy open-channel flows if vegetation elements do not interrupt the laser light sheet within vegetation, which is the situation for relatively sparse vegetation density. Our group has selected aquatic vegetation canopy flows as one of the research projects for promoting eco-hydraulics and

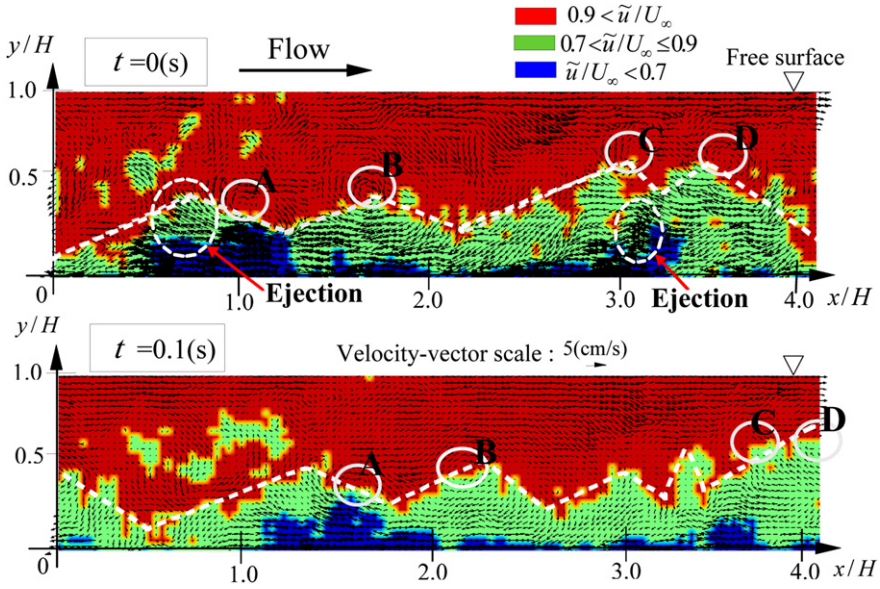

Fig. 5. Coherent vortex structure in the outer layer of open-channel flow over smooth bed ($H = 4.0$ cm, and $U_\infty = 24.0$ cm/s). The streamwise velocity vectors are subtracted by the convection velocity $U_c = 0.9U_\infty$.

environmental fluid mechanics in our new Hydraulics Laboratory after the Faculty of Engineering, Kyoto University, had moved to a new campus in 2006. More detailed information is available in Nezu and Sanjou (2008). For example, Fig. 6 shows some data comparisons of mean streamwise velocity $U(y)$ and the Reynolds stress $-\overline{uv}$ between LDA and PIV measurements in vegetated canopy open-channel flows. h is the height of vegetation elements (rigid strip plate, $h = 50$ mm height, $w = 8$ mm width and $t = 1$ mm thickness plastic plate). $U_h \equiv U(y = h)$ is the velocity at the vegetation edge ($y = h$), and is often used as a velocity-scale in mean velocity profiles. U_m is the bulk mean velocity. PIV data of mean velocity are in good agreement with LDA data even within the vegetation layer ($y/h < 1.0$), in which velocities cannot be measured easily by conventional probe devices such as hot-film, propeller current meters and electromagnetic ones. The agreement of measured Reynolds stress data between LDA and PIV measurements is also reasonable. It is found that the Reynolds stress behaves according to the linear distribution of Eq. (4) over the canopy layer ($y/h > 1.0$) in the same manner as 2-D open-channel flow over a flat bed. In contrast, the Reynolds stress is reduced significantly toward the bed within the vegetation due to the drag forces of vegetation elements. Therefore, a strong shear layer is formed near the vegetation edge ($y/h = 1.0$) and thus an inflection-point instability, i.e., Kelvin-Helmholtz instability, appears near the vegetation canopies. Consequently, typical coherent vortices are generated in the similar mechanism to mixing layers, as revealed in terrestrial canopy flows by Raupach et al. (1996).

With the advent of non-intrusive devices of LDA, ADV and PIV, intensive research on aquatic canopy flows has been opened up in the past decade. Ghisalberti and Nepf (2006) have conducted turbulence measurements over rigid and flexible vegetation canopies by using ADV although several vegetation elements had to be removed because of limitations

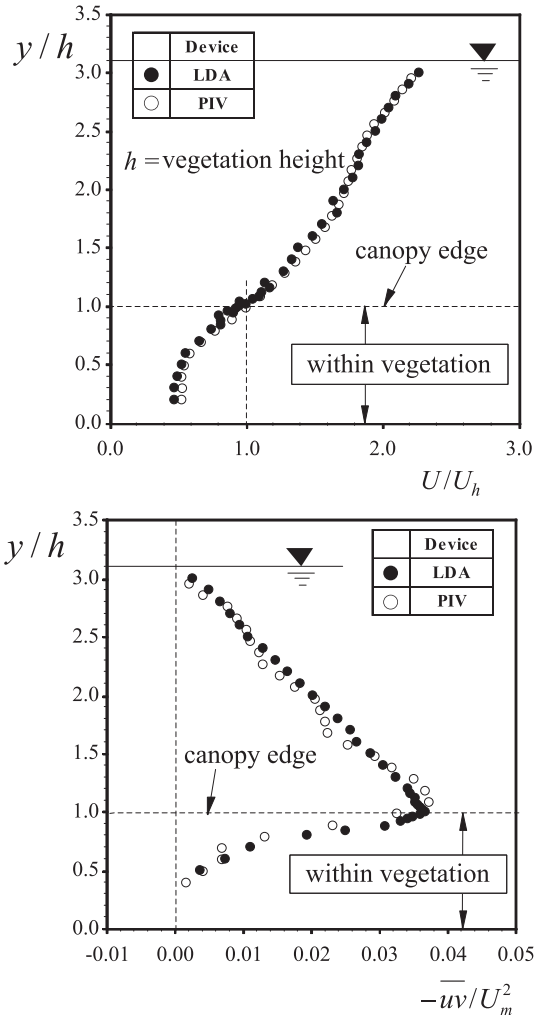

Fig. 6. Comparison of mean velocity and Reynolds stress between LDA and PIV measurements in aquatic canopy flow ($H = 15.0$ cm, $U_m = 12.0$ cm/s, and vegetation density $\lambda = 0.39$).

of ADV. They found coherent vortices such as sweeps and ejections near the canopies, and examined a validation of mixing layer analogy in aquatic canopy flows. On the other hand, Nezu and Sanjou (2008) have conducted turbulence measurements in rigid vegetated open-channel flows by using an innovative LDA (Dantec) which can measure velocities even just behind vegetation elements without any removal of vegetation. The vegetation density λ was changed 0.39 to 1.6 (densest). Nezu and Sanjou (2008) examined mean velocity profiles, turbulence intensities and Reynolds stress (such as Fig. 6), as well as turbulent kinetic energy budget and quadrant analysis, and compared them with terrestrial canopy flows. They first evaluated the dispersive stress due to space-averaging of velocity around the heterogeneity of vegetation elements in aquatic vegetated flows and confirmed the importance of double-averaging method (DAM) in obstructed flows such as gravel bed, irregular rough surfaces and vegetation, as pointed out by Nikora et al. (2007).

However, it is very difficult to reveal hydrodynamic structures of coherent vortices generated near the vegetation canopy edge by using LDA even if two or multi sets of LDAs can be used for multi-point space-time measurements. To overcome such difficulties, PIV is the most useful and powerful tool to reveal coherent vortices and the associated mass transport in vegetated open-channel flows.

Fig. 7 shows some examples of instantaneous velocity vectors $(\widetilde{u},\widetilde{v})$ and the corresponding instantaneous Reynolds stress $(-uv)$ in vegetated open-channel flow, which were measured with PIV by Nezu and Sanjou (2008). L_v is the streamwise spacing between the neighboring vegetation elements. Fig. 7(a) also shows the color contours of streamwise turbulent fluctuation component $u(x,y,t)$. An ejection motion $(u<0, v>0)$ appears just above the vegetation edge, and is followed by a sweep motion $(u>0, v<0)$ which inrushes toward the within-vegetation layer. Of particular significance is the fact that the Reynolds stress is generated most violently in the ejection motion (indicated by circle A in Fig. 7(b)) and the sweep motion (indicated by circle B). As the time passes, the ejection and sweep motions are convected downstream and appear periodically, which were revealed with PIV by Nezu and Sanjou (2008).

3.4. Turbulence structure and coherent motion in compound open-channel flows

Two-stage free-surface flows, which consist of inbank and overbank streams, are often observed in rivers during floods. Because such compound open-channel flows may cause inflection-point instabilities near the junction between the main-channel and floodplains, it is possible for coherent horizontal vortices to be generated and convected downstream. In fact, Sellin (1964) has first qualitatively visualized such horizontal vortices by the aluminum-powder method. These vortices enhance mass and momentum exchanges significantly between the high-speed main-channel and low-speed floodplain flows. The measurements of turbulence structure in compound open-channel flows have become feasible with the advent of non-intrusive measurement devices such as LDA and PIV. Tominaga and Nezu (1991) conducted accurate turbulence measurements in compound open-channel flows with a two-component LDA, and revealed the cross-sectional distributions of primary velocity, secondary currents and turbulence characteristics.

On the other hand, horizontal vortices and the associated transport phenomena may be measured more reasonably by PIV rather than LDA. For example, Nezu et al. (1999b) conducted LDA and PIV measurements in compound open-channel flows and found that a twin-horizontal-eddy structure appeared at large submergence depth, $H/D > 1.5$ (H is the flow depth, and D is the floodplain height, see Fig. 8), due to the effects of secondary currents. However, at smaller submergence depth of $H/D < 1.5$, a single eddy appears near

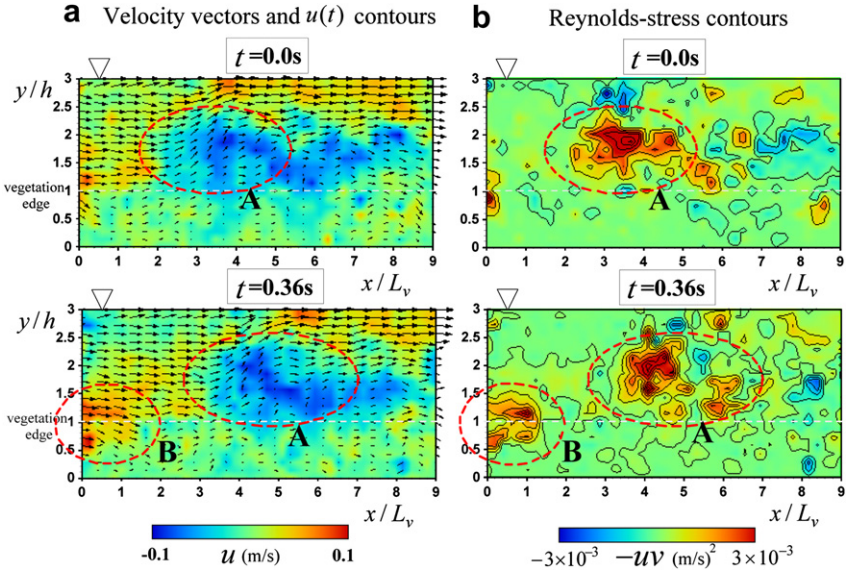

Fig. 7. Instantaneous velocity vectors $(\widetilde{u},\widetilde{v})$ and the corresponding Reynolds stress $(-uv)$ in vegetated canopy open-channel flow ($H = 15.0$ cm, $U_m = 10.0$ cm/s, and $\lambda = 0.39$). The circle zone A shows ejections, whereas B shows sweeps.

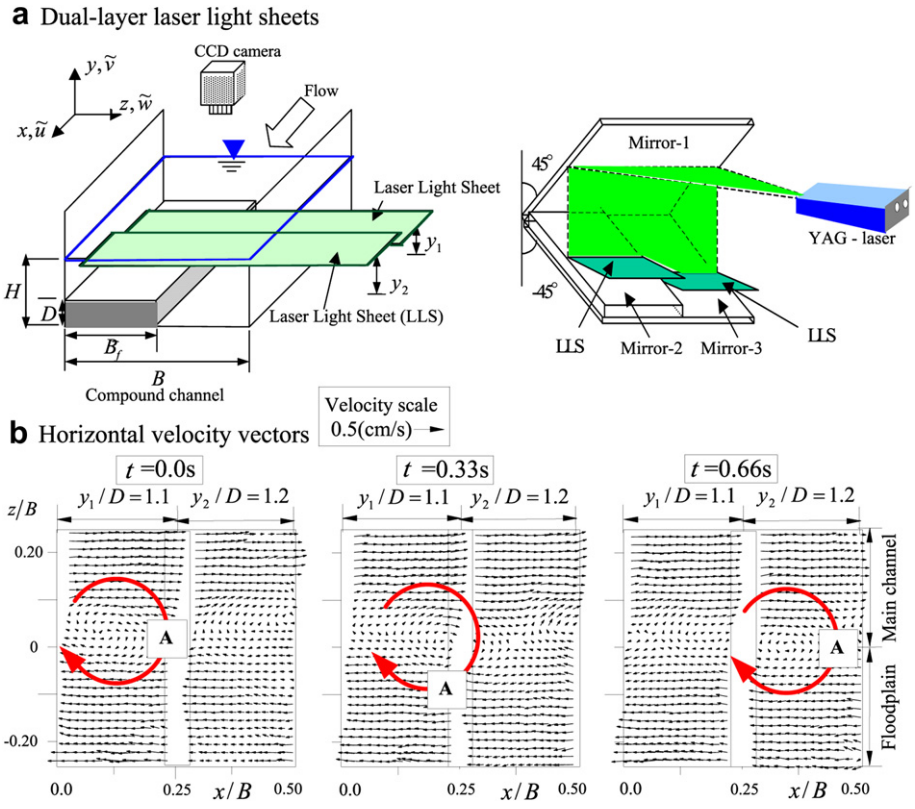

Fig. 8. (a) Measurement setup of dual-layer PIV and (b) Time-variations of horizontal velocity components $(\widetilde{u},\ \widetilde{w})$ ($H = 7.4$ cm, $D = 5.0$ cm, $B = 40$ cm, $B_f = 20$ cm, and $U_m = 10.2$ cm/s). The circle zone A shows a horizontal vortex.

the junction because of a single inflectional point in the transverse velocity distribution, as visualized by Sellin (1964). In the meanwhile, Japan and UK group have collaborated on compound open-channel flows and reviewed recent research, which is available in the IAHR monograph by Ikeda and McEwan (2009).

Later, Nezu et al. (2004a,b) developed a dual-layer PIV system, in which two different elevations y_1 and y_2 of LLS were generated using a combination of three plane mirrors as shown in Fig. 8(a). This dual-layer PIV is simple, but it may be possible to measure the 3-D structure of a vortex by changing y_1 and y_2 although the streamwise position x is of course different between the half images.

Fig. 8(b) shows the horizontal velocity vectors $(\widetilde{u},\ \widetilde{w})$ at two different elevations $y_1/D = 1.1$ (left-hand half image) and $y_2/D = 1.2$ (right-hand half image). A coherent horizontal vortex (A) observed in the upstream side of $y_1/D = 1.1$ at $t = 0.0$ s is convected in the streamwise direction, and it appears similarly in the downstream side of $y_2/D = 1.2$ at $t = 0.66$ s. These noticeable findings were also recognized in the time variations of vorticity distributions. This suggests that the coherent horizontal vortex correlates strongly between two different elevations and thus may behave in a vertical vortex-tube fashion.

Such a horizontal vortex is generated near the junction due to the inflection-point instability (shear instability) and may be convected downstream without a large variation, i.e., in a frozen-turbulence manner (Fig. 8). However, a lot of uncertainties remain concerning the convection property of horizontal vortex as well as the relation between the vortex and secondary currents.

To investigate such trajectory and deformation properties of horizontal vortices, Sanjou et al. (2010b) have developed a moving-coordinate PIV system that is moved with the same speed as the mean convection velocity of a target horizontal vortex. On considering various flow situations and scenarios of compound and meandering channel flows, we have constructed a large-scale compound channel facility ($B = 150$ cm wide and 9 m long tilting flume, maximum discharge $Q_{max} = 120$ l/s, see Fig. 9) in our new Hydraulics Laboratory, Kyoto University. This large-scale flume facility is also suitable for 3-D measurements by acoustic Doppler velocimetry (ADV) which enables us to measure all three components $(\widetilde{u},\widetilde{v},\widetilde{w})$ of instantaneous velocity although the accuracy of ADV is of course lower than that of LDA, e.g., see Sanjou et al. (2010d).

Fig. 9(a) schematized a Lagrangian PIV observation setup, in which a well-controlled carrier mounting a CMOS camera can move with a constant motor speed (variable, with a maximum speed of 50 cm/s). The digital images in the horizontal plane (40 cm × 40 cm) of the free surface were taken by a high-speed CMOS camera (1024 × 992 pixel resolution), and the time-series of instantaneous velocity components $(\widetilde{u},\widetilde{w})$ were calculated using the PIV method. The carrier speed was adjusted to be equal to the convection velocity of a target horizontal vortex. Fig. 9(b) shows some examples of instantaneous velocity vectors for a typical horizontal vortex, which are plotted at $x = 3.0$, 4.0, and 5.0 m.At

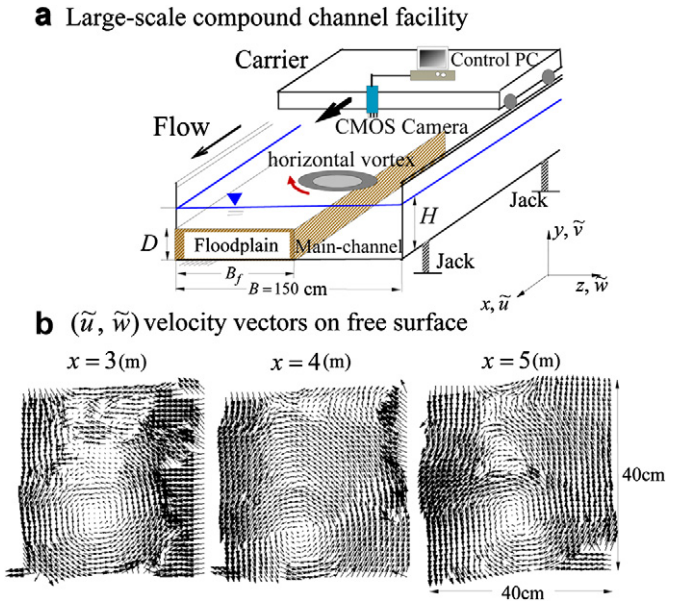

Fig. 9. (a) Lagrangian PIV placed on auto-moving carrier, (b) Instantaneous velocity vectors on free-surface at every 1.0 m in the streamwise direction ($H = 22.0$ cm, $D = 20.0$ cm cm, $B = 150$ cm, $B_f = 90$ cm, and $U_m = 15.0$ cm/s)

$x = 3.0$ m, a counter-clockwise horizontal vortex is identified near the junction zone in the main-channel. The rotation direction corresponds well to the shear instability resulting from the velocity differences between the main-channel and floodplain. This horizontal vortex is convected downstream in a frozen-turbulence manner. The spatial and temporal variations of the vortex seem to be small, and it is thus inferred that the horizontal vortex has fully developed at $x = 3.0$ m.

3.5. Direct measurements of secondary currents using PIV

It is well known that wind-induced water waves have an important relationship with large-scale secondary currents, so-called the Langmuir circulation. This circulation is observed together with high-speed and low-speed streaks on the free surface, which correspond to the convergence and divergence zones, respectively. According to CL2 theory of Langmuir circulation, e.g. see Thorpe (2004), significant quantities of mass and momentum are transported from the divergence zone toward the convergence zone near the water surface, and consequently, strong downflows are formed in the convergence zone. Furthermore, a horizontal vortex induced by spanwise variations of primary velocity is tilted by Stokes drift. These hydrodynamic properties promote the generation of Langmuir circulation, which in turn plays an essential role on 3D mass and momentum exchanges. However, it has been difficult to measure directly the cross-sectional patterns of Langmuir circulation in wind-induced open-channel flows.

Because the wind-induced water velocity is relatively small in closed water tank, it may be possible to place a waterproof high-speed camera in the water to capture the cross-sectional velocities directly. Sanjou et al. (2010a) have conducted the cross-sectional PIV in order to reveal Langmuir circulation generated by wind-induced water waves. They utilized two kinds of LLS projections, i.e., in the cross-sectional and horizontal planes. For cross-sectional PIV measurements, a high-speed CMOS camera was placed inside a waterproof acrylic box in water. The distance between the LLS and the camera was about 2 m, which was large enough to make the effects of this submerged box on the flow structure negligibly small. Fig. 10 shows an example of cross-sectional (y-z) distributions and horizontal ones (at the near-interface $y/H = 0.9$) of time-averaged velocity components, in which the spanwise velocity component W is shown by color contours. The elevation ($y/H = 0.9$) of the horizontal LLS was just below the water waves. It is found in the horizontal LLS that the divergence zone forms at the centerline, and the mass and momentum are transported toward the convergence zones near the side walls. Of particular significance is that a pair of longitudinal vortices appear clearly and they induce upflows and downflows, the positions of which coincide well with the convergence and divergence zones near the air/water interface, respectively.

4. Some advanced PIV measurements in open-channel flows

Hydraulic engineering deals with various flows in natural rivers, ocean and lakes with complicated geometry. Such geometric features as well as various sediment, roughness, aquatic plants and waves may make fluid motion and turbulence more complex and three-dimensional (3D). It may be difficult for standard PIV as described above to apply to these various kinds of complex flows even in laboratory flumes. To overcome these difficulties, a lot of techniques of PIV measurements have been advanced and improved including the PIV hardware setup and the methods of calculation for velocity vectors. Nowadays, 3D stereoscopic PIV, color-coded PIV, multiphase PIV and temperature/concentration measurements with PIV are available and applied in a wide variety of application fields, especially in mechanical engineering, e.g. see Schroeder and Willert (2008) and Ruck (2011).Our group developed some advanced PIV and applied to complex situations of open-channel flows.

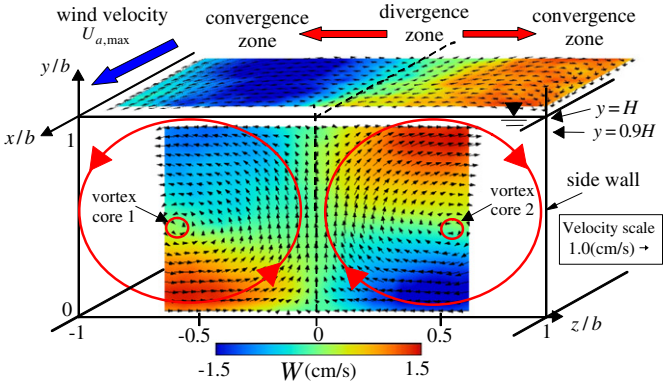

Fig. 10. Langmuir circulation visualized by cross-sectional and horizontal PIV measurements in wind-induced water waves (flow depth $H = 20.0$ cm, half channel width $b = B/2 = 20.0$ cm, and wind velocity $U_{a,max} = 7.78$ m/s).

4.1. Simultaneous measurements of free-surface elevations and velocity components

When wind develops over a water surface, water waves and turbulence are generated by the interfacial shear stress. In particular, coherent turbulence will promote significant mass and momentum transport beneath the air/water interface in ocean and lakes. Thus, it is very important in global environmental problems to explain coherent structures and the associated transport phenomena in wind-driven water waves. A lot of studies on such challenging topics have been conducted by non-intrusive devices such as LDA and ultrasonic depth gauges, e.g. see Nezu et al. (2003). However, uncertainties remain concerning the effects of wave phases on coherent motion such as ejections/sweeps and the associated gas transfer. Therefore, we have developed a specially designed PIV system that can measure velocity components and surface-elevation fluctuations simultaneously by using two sets of high-speed cameras to reveal the coherent structures in an interfacial shear layer.

The experiments were conducted in a 16 m long, 40 cm wide and 50 cm high glass-made wind-tunnel flume (same facility as used in Fig. 10). In this flume, the airflow was generated over the free surface by a speed-controlled wind fan. A 2W laser light sheet was projected from the flume bottom and illuminated the $x - y$ vertical plane at the channel center in the same manner as shown in Fig. 1. To measure the velocity components $(\widetilde{u}(t), \widetilde{v}(t))$ and the free-surface elevation $\eta(t)$ simultaneously, two sets of high-speed cameras (1024 × 992 pixels, 500 frames/s) were synchronized for PIV measurements and the free-surface capture. To detect the air–water interface accurately, Rhodamine-B was dissolved in the flume water to improve the clarity near the interface between air and water.

Using the brightness data $B(x,y)$ of images near the air/water interface, the brightness gradient $\partial B/\partial y$ in the vertical direction was calculated, and its maximum point was searched at each location in the x direction. This maximum point is considered as a free-surface elevation $\eta(x,t)$, as discussed by Sanjou et al. (2010c). Fig. 11 shows some examples of instantaneous velocity vectors $(\widetilde{u}(t), \widetilde{v}(t))$ and the corresponding free-surface elevation $\eta(x,t)$, in which the $\widetilde{u}$ component is also shown by color contours for visible motion. It is seen that the crest/trough of waves are convected downstream with time. The downflows appear on the back side of the crest, whereas the upflows appear on the front side. In contrast, the downflows and upflows are observed on the forward and backward sides of the trough, respectively. From the $\widetilde{u}$ contours, it is found that high velocity zones are located near the crest, whereas the return-flow zones are formed near the trough. From these fundamental data of velocity vectors and the associated free-surface profiles, various phase analyses of turbulence characteristics and the coherent structures can be examined. More detailed information is available in Sanjou et al. (2010c).

4.2. Three-dimensional PIV

PIV measurements are very useful to understand time-variations of instantaneous velocity vectors in space, and thus, coherent structures such as bursting phenomena and horizontal vortices have been investigated intensively. However, a standard PIV is only capable of obtaining two velocity components in a plane, and the out-of-plane component cannot be measured. Furthermore, the in-plane components may be measured less accurately in larger secondary currents, i.e., stronger 3D turbulent flows. To overcome these difficulties, various developments of 3D PIV that can measure all three components of velocity have been conducted in the fluid engineering community. Stereoscopic PIV is often used as 3D PIV measurements, in which additional PIV recordings are made from different view directions using pairs of cameras. Detailed information on principles, image reconstruction and calibration procedures of stereoscopic PIV is available, e.g., in Schroeder and Willert (2008).

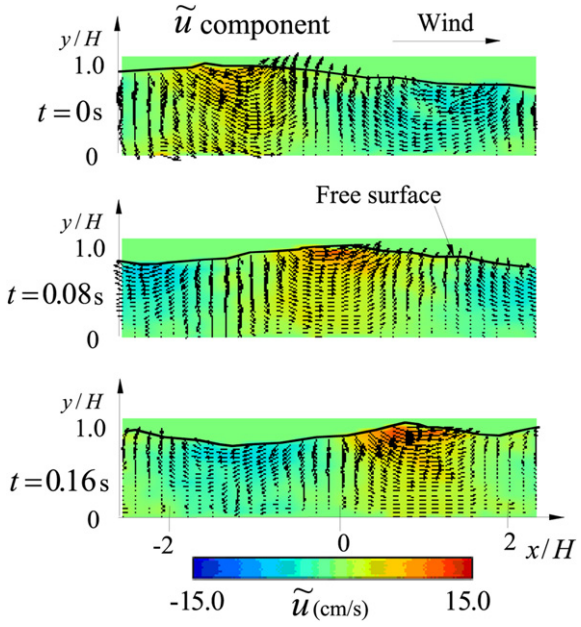

Fig. 11. Instantaneous velocity vectors and free-surface shape obtained by dual-camera system in wind-induced water waves (H = 4.0 cm, and $U_{a,\max}$ = 6.8 m/s).

Although stereoscopic PIV can measure all three components of velocity in a plane, it may be difficult to measure instantaneous velocity vectors in 3D fluid volume. To do so, a multi-layer scanning PIV system has been developed by several researchers. An idea of 3D imaging techniques consists of scanning laser light sheets (LLS) using a well-controlled polygon mirror or a rotating drum. Although the scanning LLS is much more complicated than the classic fixed LLS, the former can measure two components and even all three components of velocity in 3D fluid volume. More detailed information is available in Kelso and Delo (2000). The other fantastic idea may be color-coded tomography, in which a multi-color laser tomography (MLT) is used for single camera that may be conducted more easily than multi-cameras for stereoscopic PIV. In such a MLT, two velocity components are evaluated from the detected image plane and the third one will be derived from the color. More detailed information is available in Ruck (2011).

Since the 2000's, our group has also intended to develop a multi-layer scanning PIV system to investigate horizontal vortices in the water volume near the junction of compound open-channel flows because a classical fixed LLS such as used in Fig. 8 has a limitation of utility, especially the latter cannot measure velocities in the same water volume simultaneously. As a result, Nezu et al. (2005) designed a multi-layer scanning LLS instrument and applied it to an open-channel flume, as shown in Fig. 12(a), in which x, y and z are the streamwise, vertical and spanwise coordinates, respectively. Three-layer LLSs at different adjusted elevations were projected horizontally into the flume using a well-controlled rotating beam splitter. This beam splitter had three pairs of double arms attaching the adjustable plane mirrors on the tip. The PIV analyses for three different layers in a water volume were conducted based on two sets of digital images that were illuminated by the neighboring same-elevation mirrors. A 2 W Ar-ion laser light was used for the scanning LLS. In total, six arms were used with each mirror placed at a constant angle span of 60° (i.e., 360°/6). The speed of the beam rotation was 10 Hz, and thus the time lag of the neighboring LLS was $1/(6 \times 10) = 0.0167$ s. Nylon-12 seeding particles (100 μm diameter and specific density of 1.02) were uniformly scattered in the flume water. The distance Δy between the neighboring LLSs was adjusted accurately to $\Delta y = 5$ mm (Fig. 12(a)). Digital images in the horizontal planes at three different elevations were taken almost simultaneously at a maximum frame rate of 250 Hz by a high-speed CCD camera placed above the free surface. The sampling duration was 60 s for all cases. The more the laser light sheets are split and projected, the more detailed information is available in 3D scanning PIV. The maximum number of the beam splitters was designed as 16 in the present system.

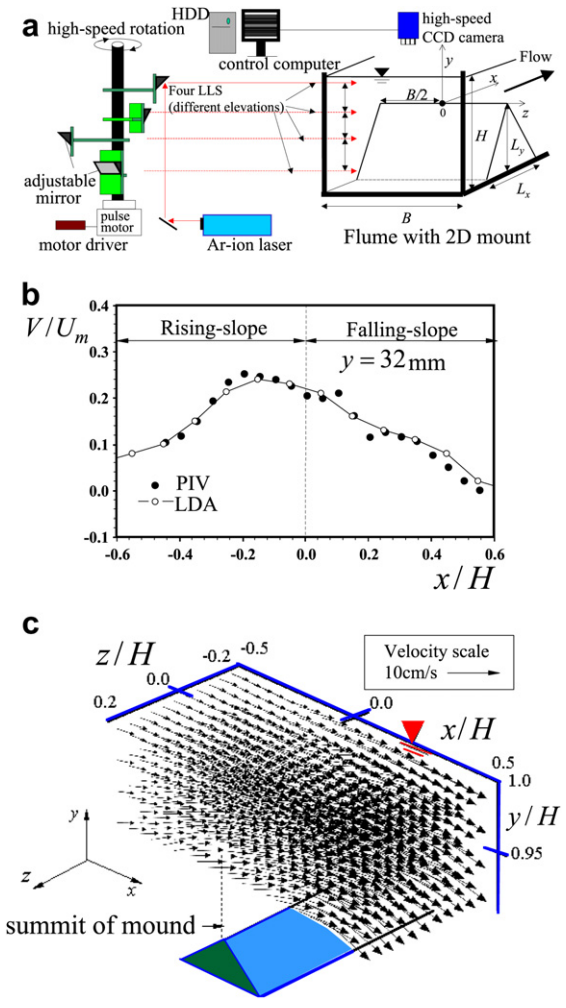

Fig. 12. Multi-layer scanning PIV measurements in mount open-channel flows, (a) Experimental setup, (b) Examination of scanning PIV accuracy by comparison with LDA data and (c) 3-D instantaneous velocity vectors in the measured volume ($H = 11.0$ cm, and $U_m = 3.4$ cm/s)

Nezu et al. (2005) examined the measurement accuracy of the present scanning 3D PIV in a 2D mount obstructed open-channel flow (Fig. 12(a)), in which an upflow ($V > 0$) and downflow ($V < 0$) appear comparatively strongly. The PIV data were compared with LDA data, by which U and V were directly measured accurately. Fig. 12(b) shows an example of streamwise distribution of time-averaged vertical velocity component $V(x)$ at a fixed elevation. The PIV data of V was evaluated from the PIV-measured horizontal velocity components (U, W) using the continuity equation, in which the boundary condition was assumed to $V = 0$ at the free-surface $y = H$ because of no water waves. It is found that the values of $V(x)$ attain a peak just before the top of the mount, and the PIV data are in good agreement with LDA data. It should be noticed that the scanning PIV can obtain 3D instantaneous velocity vectors in the scanning fluid volume by calculating the out-of-plane velocity component with the continuity equation. Fig. 12(c) shows an example of such 3D instantaneous velocity vectors near the mount flow. Sanjou and Nezu (2009) have applied the multi-layer scanning PIV system to meandering compound open-channel flows in order to examine the relation between horizontal vortices and secondary currents.

4.3. Fluid-particle interaction and sediment concentration in sediment-laden flows

The discrimination method between fluid and sediment particles has been developed by several researchers, as mentioned in 2.4. Noguchi and Nezu (2009) have improved the particle-size discrimination method of Nezu and Azuma (2004) using a high-resolution CMOS camera (1280 × 1024 pixels, Dantec) and utilized the PIV for fluid velocity instead of PTV although the sediment particles were of course measured by PTV. To conduct PIV/PTV measurements reasonably, the occupied area of sediment particles was projected about 100 times larger than that of the fluid tracer (Nylon-12, specific density = 1.02 and diameter = 25 μm). The sediment concentration was calculated by counting the number of sediment particles in PTV images.

Fig. 13 shows some examples of time-series of instantaneous Reynolds stress contours $-uv/U_*^2$ and the associated sediment concentration $\widetilde{c}(x,t)$ near the bed. A typical ejection

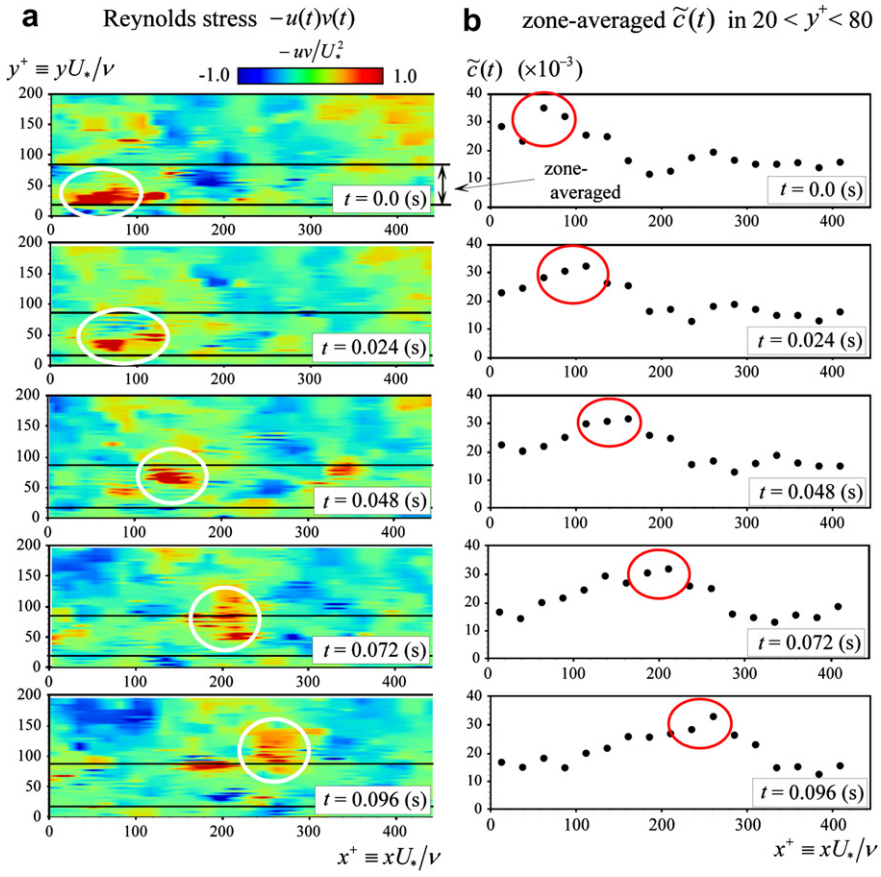

Fig. 13. Time-series of (a) instantaneous Reynolds stress $-u(t)v(t)$ and (b) the associated sediment concentration $\widetilde{c}(t)$ in sediment-laden open-channel flow ($H = 5.0$ cm, and $U_m = 30.0$ cm/s). The sediment particles have all the density $\rho_p = 1.2$ and diameter $d_p = 0.25$ mm.

motion (indicated by white circle) occurs at $t = 0$ s near the bed. This area of positive Reynolds stress values is convected downstream with a subsequent rise toward the free surface. The plotted data of $\widetilde{c}(x,t)$ is the zone-averaged concentration in the region of $20 < y^+ < 80$ (indicated by black line in Fig. 13) for each x-position. When the ejection motion occurred at $t = 0.0$ s, the particle concentration became larger (indicated by red circle). This implies that the high-concentration area is transported by the ejection motion. Noguchi and Nezu (2009) further examined the conditional analysis of the sediment flux $\overline{cv}$ in the quadrant theory, and found that the largest contribution to $\overline{cv}$ is the ejection motion. Such PIV/PTV measurements of sediment-laden flows will be contributory to reveal the relation between coherent structures and particle concentration and to understand the mechanism of sediment transport in open-channel flows. Similar investigations are available in Breugem and Uijttewaal (2006), Muste et al. (2009) and others.

4.4. Simultaneous measurements of velocity and scalar concentration using PIV and LIF

In aquatic vegetated flows and various other flow situations, it is suggested strongly that large-scale coherent vortices govern mass and momentum exchanges between the over- and within-vegetation layers. Therefore, it is very important for the river environment to reveal such a mass transport mechanism in vegetated open-channel flows. However, it has been difficult to measure the distributions of scalar concentration such as mass and temperature within the vegetation layer in aquatic flows.

Fortunately, the recently-developed laser-induced fluorescence (LIF) provides a non-intrusive method of high-resolution measurements of mass concentration in water channels. The dependence of fluorescence on dye concentration enables us to measure concentration fluctuations in water by the use of Rhodamine-B, for which fluorescent quantum efficiency increases linearly with concentration. Measuring the concentration field with the LIF technique involves exciting a fluorescent dye tracer (Rhodamine-B), with light at a wavelength within its absorption range. The dye re-emits a longer-wavelength light. After careful calibration, the digital images of the instantaneous emitted intensity are converted to the concentration field $\widetilde{c}(x,y,t)$. If the LIF is successfully used to combine with PIV, the instantaneous velocity vectors $(\widetilde{u}(x,y,t),\widetilde{v}(x,y,t))$ and dye concentration $\widetilde{c}(x,y,t)$ can be measured simultaneously in space and time, which are very challenging topics to investigate the relation between the coherent vortices and the associated mass transport in aquatic flows. These non-intrusive techniques are superior to probe (point) measurements with intrusive devices even if the latter may be more accurate than the former. Borg et al. (2001) have successfully conducted simultaneous

velocity and dye concentration measurements in a turbulent jet with a combination of PIV and LIF. On the other hand, Herlina and Jirka (2008) have conducted simultaneous measurements of velocity and dissolved oxygen (DO) concentration with a combination of PIV and LIF near the air–water interface induced by oscillating grid turbulence.

In a similar manner, our group of Okamoto et al. (2010) has conducted such challenging simultaneous measurements with a combination of PIV and LIF in aquatic vegetation canopy flow. Rhodamine-B dye was injected through a stainless nozzle into the flow near the vegetation. The injection speed of the dye was controlled carefully to coincide with the streamwise flow velocity at the same elevation. Two sets of high-speed CMOS cameras (1024 × 992 pixels resolution) were placed on the side of flume (channel width $B = 40$ cm). One camera was used for PIV measurements and the other was used for LIF measurements. These cameras were controlled simultaneously by using the trigger signals of a pulse generator. A 2W YAG laser light sheet (LLS) was projected into the water. The illuminated plane was captured by these cameras with 200 Hz frame rate and 45 s sampling time. The time-series of instantaneous velocities $(\widetilde{u}, \widetilde{v})$ were obtained by PIV algorithm. The reflection wavelength of tracer particles was 537 nm, and in contrast, the fluorescence of dye induced by the LLS had a 580 nm wavelength. So, only the image of the dye could be taken by one camera with a sharp high-pass filter (>550 nm).

Fig. 14(a) shows some examples of distributions of the instantaneous Reynolds stress $-u(t)v(t)$, which were obtained by PIV. Similar coherent structures such as sweeps and ejections to those of Fig. 7 are observed clearly in Fig. 14 although both hydraulic conditions are slightly different to each other. Fig. 14(b) shows the corresponding simultaneous concentration field $\widetilde{c}(x, y, t)$ by LIF, and reveals a high spatial variability of the instantaneous concentration. At $t = 0.0$(s), a sweep motion appears near the vegetation edge. It is observed that the large distribution of the instantaneous concentration is transported toward the within-vegetation layer by this sweep motion. At $t = 4.8$(s), an ejection motion appears and causes the local increase of the concentration above the vegetation. At $t = 7.5$(s), the ejection motion is convected downstream and the other sweep motion appears at the upstream side. The individual filaments of the dye concentration are observed clearly and the highly intermittent nature of the dye plume is found in Fig. 14(b). These images also show that the locally-high distributions of dye concentration correspond well to the coherent structure zones. This confirms that large-scale organized motions govern the mass transport in aquatic vegetated open-channel flows.

Of particular significance is the evaluation of turbulent scalar flux of a passive contaminant. The PIV-LIF measurements will allow us to evaluate the local covariance between the concentration and velocity fluctuations, $\overline{uc}$ and $\overline{vc}$. Our recent investigation found that the high distribution of concentration ($c > 0$) is transported upward by the ejection motion ($u < 0$) over the vegetation layer. In contrast, $\overline{uc}$ becomes positive within the vegetation layer, which implies that the sweep motion ($u > 0$) transports the dye concentration into the vegetation layer ($c > 0$). More detailed information is available in Okamoto et al. (2010).

For flexible vegetation, it is necessary to investigate an interaction between fluid motion and vegetation motion. Nezu and Okamoto (2010) conducted simultaneous measurements

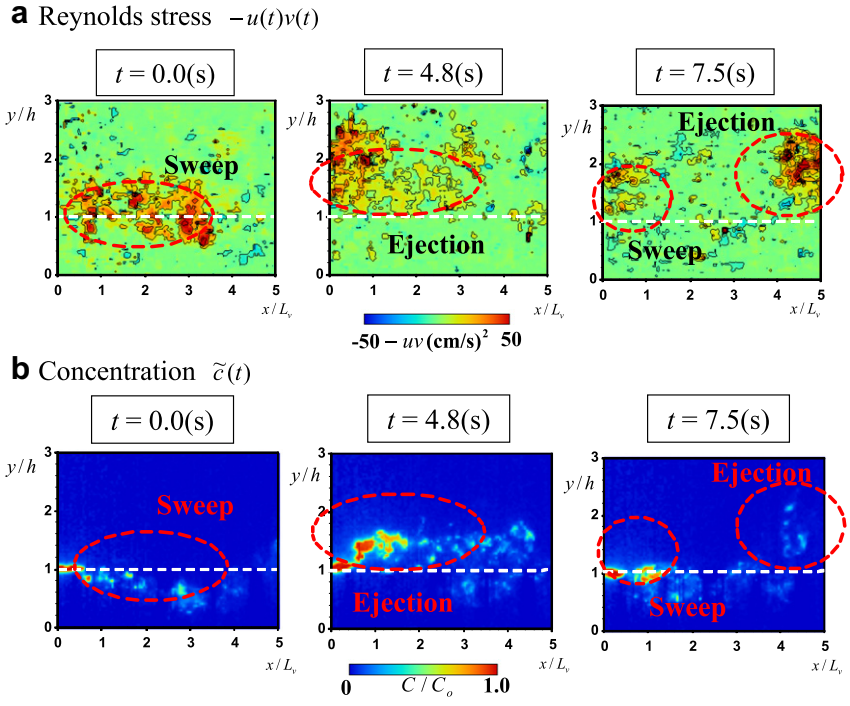

Fig. 14. Simultaneous measurements of (a) instantaneous Reynolds stress by PIV and (c) instantaneous dye concentration by LIF in vegetated open-channel flow ($H = 15.0$ cm, $U_m = 12.0$ cm/s, and vegetation density $\lambda = 0.39$). (a) Reynolds stress $-u(t)v(t)$. (b) Concentration $\widetilde{c}(t)$.

of velocity and plant motion in open-channel flows with flexible vegetation. The fluid velocity was measured with PIV and the plant motion was simultaneously measured with PTV by applying our discriminator PIV/PTV. It is also possible to measure fluid velocity, plant motion and dye concentration simultaneously by a combination of PIV-PTV-LIF in order to reveal mass transport in flexible vegetated open-channel flows.

5. Concluding remarks

PIV/PTV technique is one of the most powerful and non-intrusive measurements in hydro-sciences as well as fluid engineering community. According to our experiences of PIV/PTV measurements, the present article highlighted the applications of PIV/PTV to open-channel flows with various flow situations, which have been conducted for the past decade in Hydraulics Laboratory of Kyoto University. In Section 2, we introduced our experimental setup and PIV/PTV algorithm. In particular, a discrimination method between fluid and sediment particles was proposed. In Section 3, we applied the PIV measurements to reveal turbulence characteristics and coherent structures over smooth beds in open-channel flows. It was recognized that the PIV data were in good agreement with LDA data in the second-order turbulence statistics at least, the latter of which is expected to be the most accurate and reliable one in velocity measurement devices. PIV is also very powerful to examine coherent structures such as ejections and sweeps over rough beds and other complex flows. In this study, vegetation elements were chosen as a kind of roughness elements, and PIV measurements were applied to vegetated open-channel flows. For complex flow situations, various applications of PIV were conducted in compound open-channel flows and wind-induced water waves to reveal coherent vortices.

In Section 4, we discussed some advanced PIV measurements in open-channel flows. The free-surface-elevation fluctuations and velocity components were measured simultaneously with two sets of cameras to examine phase-averaged quantities of turbulence. 3D PIV is one of the most innovative techniques to be developed in the fluid measurement community. We have developed a multi-layer scanning PIV and applied to compound open-channel flows. Our discriminator PIV/PTV was applied successfully to sediment-laden open-channel flows and revealed the fluid/particle interaction and the relationship between coherent structures and sediment concentration. Finally, we conducted simultaneous measurements of velocity and dye concentration using both PIV and LIF in vegetated open-channel flow, which enabled us to examine turbulent scalar flux of a passive contaminant.

The above-mentioned measurements with PIV/PTV were conducted in well-controlled laboratory flumes. It is also expected that these applications and information may be extended to conduct field measurements in rivers by the use of relevant PIV (e.g., LSPIV) although the present LSPIV may be difficult to measure velocities below the free surface of natural rivers even using innovative video systems. More detailed information on LSPIV will be available in this JHER Special Issue, as announced by Fujita et al. (2009).

On the other hand, such a laboratory PIV mentioned in this study will be much more innovated to reveal 3D structures in complex unsteady flows. One of the most challenging techniques may be tomographic PIV, which combines the favorable characteristics of stereoscopic PIV and medical tomography. Scarano (2010) reviewed such a tomographic PIV and introduced some examples (four cameras were used) in vortex shedding phenomena. In contrast, Ruck (2011) developed a color-coded tomographic PIV, in which multi-color laser tomography (MLT) system and single camera are used. These innovative tomographic PIV will be able to be applied to turbulence measurements in open-channel flows with complex geometry in near future.

Acknowledgments

Professor V. Nikora, University of Aberdeen, kindly invited the author (I. Nezu) to write the present review article on the basis of his experiences and achievements. The authors would like very much to thank Professor Nikora for this kind opportunity and encouragement. Dr. Stuart Cameron under Professor Nikora kindly helped with checking English of the original manuscript, which is greatly acknowledged. The authors also appreciate the valuable comments offered by anonymous reviewers.

References

Acarlar, M.S., Smith, C.R., 1987. A study of hairpin vortices in a laminar boundary layer. J. Fluid Mech. 175, 1−83.

Adrian, R.J., 1986. Multi-point optical measurements of simultaneous vectors in an unsteady flow-a review. Int. J. Heat Fluid Flow 7, 127−145.

Adrian, R.J., 1991. Particle-imaging techniques for experimental fluid mechanics. Annu. Rev. Fluid Mech. 23, 261−304.

Adrian, R.J., Meinhart, C.D., Tomkins, C.D., 2000. Vortex organization in the outer region of the turbulent boundary layer. J. Fluid Mech. 422, 1−54.

Borg, A., Bolinder, J., Fuchs, L., 2001. Simultaneous velocity and concentration measurements in the near field of a turbulent low-pressure jet by digital particle image velocimetry − planar laser induced fluorescence. Exp. Fluids 31, 140−152.

Breugem, W.A., Uijttewaal, W.S.J., 2006. A PIV/PTV experiment on sediment transport in a horizontal open channel flow, river flow 2006. In: Ferreira, R. M.L., et al. (Eds.). Taylor & Francis, pp. 789−798.

Fujita, I., Muste, M., Kruger, A., 1998. Large-scale particle image velocimetry for flow analysis in hydraulic engineering applications. J. Hydraul Res. 36, 397−414.

Fujita, I., Muste, M., Hauet, A., 2009. LSPIV − a Powerful Tool for Measurements in Hydrosciences. Hydrolink, IAHR, pp. 72−73.

Ghisalberti, M., Nepf, H., 2006. The structure of the shear layer in flows over rigid and flexible canopies. Environ. Fluid Mech. 6, 277−301.

Hart, D.P., 2000. PIV error correlation. Exp. Fluids 29, 13−22.

Herlina, Jirka, G.H., 2008. Experiments on gas transfer at the air-water interface induced by oscillating grid turbulence. J. Fluid Mech. 594, 183−208.

Hurther, D., Lemmin, U., Terray, E.A., 2007. Turbulent transport in the outer region of rough-wall open-channel flows: the contribution of large coherent shear stress structures (LC3S). J. Fluid Mech. 574, 465−493.

Ikeda, S., McEwan, I.K. (eds.), Flow and Sediment Transport in Compound Channels, the Experiences of Japanese and UK Research, IAHR Monograph, IAHR.

Kadota, A., Aragao, R., Suzuki, K., 2007. Visualization of flow pattern around two-in-tandem cylinders. In: Proc. of 32nd IAHR Congress of Venice No. 534 (CD-ROM).

Kelso, R.M., Delo, C., 2000. Three-dimensional imaging (Chp. 10), flow visualization. In: Smits, A.J., Lim, T.T. (Eds.). Imperial College Press.

Kobayashi, T. (Ed.), 2002. Handbook of Particle Image Velocimetry. Visualization Society of Japan, Morikita Pub (in Japanese).

Muste, M., 2002. Sources of bias errors in flume experiments on suspended-sediment transport. J. Hydraul Res. 40, 695−708.

Muste, M., Yu, K., Fujita, I., Ettema, R., 2009. Two-phase flow insights into open-channel flows with suspended particles of different densities. Environ. Fluid Mech. 9, 161−186.

Nezu, I., Azuma, R., 2004. Turbulence characteristics and interaction between particles and fluid in particle-laden open-channel flows. J. Hydraul Eng. 130, 988−1001.

Nezu, I., Nakagawa, H., 1993. Turbulence in Open-channel Flows. In: IAHR Monograph. Balkema, Rotterdam.

Nezu, I., Okamoto, T., 2010. Simultaneous measurements of velocity and plant motion in open-channel flows with flexible vegetations, environmental hydraulics. In: Christodoulou, G.C., Stamou, A.I. (Eds.). Taylor & Francis, pp. 209−214.

Nezu, I., Sanjou, M., 2008. Turbulence structure and coherent motion in vegetated canopy open-channel flows. J. Hydro-Environment Res. 2, 62−90.

Nezu, I., Esaki, K., Onitsuka, K., 1999a. Interaction between turbulence structure and bed-load transport in open-channel flows, hydraulic modeling. In: Singh, V.P., et al. (Eds.). Water Resources Pub, pp. 63−76.

Nezu, I., Onitsuka, K., Iketani, K., 1999b. Coherent horizontal vortices in compound open-channel flows, hydraulic modeling. In: Singh, V.P., et al. (Eds.). Water Resources Pub, pp. 17−32.

Nezu, I., Yoshida, K., Ikeda, D., 2003. Experimental study on mutual turbulent structures across air−water interface in wind-induced water waves by synchronous LDA measurements. J. Hydrosci Hydraul Eng. JSCE 21, 63−70.

Nezu, I., Sanjou, M., Goto, K., 2004a. Transition process of coherent vortices in depth-varying unsteady compound open-channel flows, shallow flows. In: Jirka, G.H., Uijttewaal, W.S.J. (Eds.). Balkema, pp. 251−258.

Nezu, I., Sanjou, M., Goto, K., 2004b. 3-D coherent structure of horizontal vortices in compound open-channel flows. In: Proc. of 6th Int. Conf. on Hydro-Sciences and Eng. (ICHE). IAHR, Brisbane, 10 pp on CD-ROM.

Nezu, I., Sanjou, M., Kamiya, A., 2005. Development of multi-layer laser-scanning PIV and applications to hydraulic engineering. In: Proc. of 31st IAHR Congress, Seoul, 10 pp on CD-ROM.

Nikora, V., McEwan, I., McLean, S., Coleman, S., Pokrajac, D., Walters, R., 2007. Double-averaging concept for rough-bed open-channel and overland flows: theoretical background. J. Hydraul Eng. 133, 873−883.

Nino, Y., Garcia, M.H., 1996. Experiments on particle-turbulence interactions in the near-wall region of an open channel flow: implications for sediment transport. J. Fluid Mech. 326, 285−319.

Noguchi, K., Nezu, I., 2009. Particles-turbulence interaction and local particle concentration in sediment-laden open-channel flows. J. Hydro-Environment Res. 3, 54−68.

Okamoto, K., Hassan, Y.A., Schmidt, W.D., 1995. New tracking algorithm for particle image velocimetry. Exp. Fluids 19, 342−347.

Okamoto, T., Nezu, I., Katayama, A., 2010. Simultaneous measurements of concentration and velocity with combined PIV and planar LIF in vegetated open-channel flows. In: Dittrich, A., et al. (Eds.), Proc. of River Flow 2010, pp. 487−494. Braunschweig.

Raffel, M., Willert, C., Wereley, S., Kompenhans, J., 2007. Particle Image Velocimetry. Springer.

Raupach, M.R., Finnigan, J.J., Brunet, Y., 1996. Coherent eddies and turbulence in vegetation canopies: the mixing-layer analogy. Boundary-Layer Meteorol. 78, 351−382.

Ruck, B., 2011. Colour-coded tomography in fluid mechanics. Opt. Laser Technol. 43, 375−380.

Sanjou, M., Nezu, I., 2009. Turbulence structure and coherent motion in meandering compound open-channel flows. J. Hydraul Res. 47, 598−610.

Sanjou, M., Nezu, I., 2010. Effects of free-surface shear on coherent hairpin vortex generated near flume bed. In: Proc. of 17th IAHR-APD Congress Auckland, No. 1c0289 (USB-ROM).

Sanjou, M., Nezu, I., Akiya, Y., 2010a. Experimental study on Langmuir circulation generated by wind-induced water waves. In: Proc. of 8th Int. Symp. on Ecohydraulics 2010, pp. 1146−1151. Seoul.

Sanjou, M., Nezu, I., Suzuki, S., 2010b. PIV measurements of horizontal vortex in large-scale compound open-channel flow. In: Proc. of 17th IAHR-APD Congress Auckland, No. 1c028 (USB-ROM).

Sanjou, M., Nezu, I., Toda, A., 2010c. Coherent turbulence structure generated by wind-induced water waves. In: Dittrich, A., et al. (Eds.), Proc. of River Flow 2010, pp. 1673−1680. Braunschweig.

Sanjou, M., Nezu, I., Itai, K., 2010d. Space-time correlation and momentum exchanges in compound open-channel flow by simultaneous measurements of two-sets of ADVs. In: Dittrich, A., et al. (Eds.), Proc. of River Flow 2010, pp. 495−502. Braunschweig.

Scarano, F., 2010. 3D Optical Diagnostics from Aerodynamics to Hydraulics. Hydrolink, IAHR, pp. 62−65.

Schroeder, A., Willert, C.E. (Eds.), 2008. Particle Image Velocimetry; New Developments and Recent Applications. Springer.

Sellin, R.H.J., 1964. A laboratory investigation into the interaction between the flow in the channel of a river and that over its floodplain. La Houille Blanche 7, 793−802.

Thorpe, S., 2004. Langmuir circulations. Annu. Rev. Fluid Mech. 36, 55−79.

Tominaga, A., Nezu, I., 1991. Turbulent structures in compound open-channel flow. J. Hydraul Eng. 117, 21−41.

Tomkins, C.D., Adrian, R.J., 2003. Spanwise structure and scale growth in turbulent boundary layers. J. Fluid Mech. 490, 37−74.